EPJ Web of Conferences **377**, 05003 (2026) https://doi.org/10.1051/epjconf/202637705003
IPS 2026

Energy Efficiency Improvement in a Hybrid PV-TEG System with Finned Aluminum Heatsinks

Syafrima Wahyu[1*], *Nur Rahma* Hidayanti[1], *Puji* Suharmanto[2], *Temon* Sujadi[3], and *Ahmad* Fitra Ritonga[4]

[1]Department of Physics, Universitas Negeri Jakarta, Jl. Rawamangun Muka, Jakarta 13220, Indonesia
[2]Ph.D Management Business Graduate School, Universiti Tun Abdul Razak, Kuala Lumpur, Malaysia
[3]PT Solar Energy Power, Jl. Prapanca 2, Perum Grand Residence City, Cijengkol, Setu Bekasi, 17320, Indonesia
[4]Department of Physics Education, Universitas Sriwijaya, Jl. Raya Palembang-Prabumulih, Sumatera Selatan, 30862, Indonesia

Abstract. Hybrid photovoltaic-thermoelectric generator (PV-TEG) systems can recover waste heat from PV modules, but performance relies on maintaining a sufficient temperature difference (ΔT) across thermoelectric modules. Excessive PV temperature reduces output and limits TEG benefits, making thermal management critical. This study evaluated finned aluminum heatsinks on a hybrid PV-TEG system using two 5 Wp monocrystalline panels with sixteen TEC1-12706 modules, eight connected in series beneath each panel. Three configurations were tested: no heatsink, 4-fin, and 11-fin heatsinks. Experiments were conducted under 100 W LED illumination with data logged every 2 min for 2 h. Voltage, current, and temperature were measured via INA219 and DS18B20 sensors connected to an Arduino acquisition system, and overall efficiency calculated from output power and incident irradiance. Results showed that heatsinks improved efficiency from 0.64% (no-heatsink) to 0.83% (4-fin) and 0.87% (11-fin). The 11-fin configuration produced the highest average power (0.2148 W) and largest ΔT (11.57 °C). Increasing fin count enhances heat dissipation, lowers TEG cold-side temperature, and improves overall electrical output. These findings provide practical guidance for the design and optimization of small-scale PV-TEG systems, supporting enhanced energy recovery and efficient thermal management in future applications.

1 Introduction

The global energy crisis and the need to reduce carbon emissions have intensified research on renewable energy technologies, with solar energy attracting particular attention because of its vast potential and wide availability. Photovoltaic (PV) systems directly convert solar radiation into electricity and offer important advantages such as sustainability, modularity, and low operational maintenance. However, the principal limitation of PV technology

* Corresponding author: syafrimawahyu@unj.ac.id

remains its relatively low conversion efficiency, as only a fraction of the absorbed solar energy is converted into electrical power while the remainder is dissipated as heat. As PV cell temperature increases, the electrical performance of the module declines, particularly through a reduction in output voltage and overall power. Consequently, effective thermal-management strategies are required to maintain stable and efficient PV operation [1–3].

One promising approach to utilizing PV waste heat is the integration of thermoelectric generators (TEGs), which operate according to the Seebeck effect and convert a temperature difference directly into electrical energy. When mounted on the rear surface of a PV panel, TEG modules can harvest part of the heat rejected by the PV layer and generate supplementary electrical power. Such a hybrid PV-TEG architecture therefore enables the simultaneous use of photon energy and thermal energy within a single solar-energy platform. Recent studies have shown that hybridization can improve overall system output. Reviews and experimental investigations have reported that PV-TEG integration can enhance total energy utilization, especially when supported by appropriate thermal-management methods that preserve a sufficient temperature gradient across the TEG [4,5].

Despite this potential, the performance gain of PV-TEG systems depends strongly on maintaining a low cold-side temperature so that a sufficiently large temperature difference, ΔT, can be sustained across the thermoelectric modules. For this reason, numerous cooling strategies have been explored, ranging from active methods such as liquid circulation, heat pipes, and phase-change materials to simpler passive or low-complexity methods such as fins, thermally selective surfaces, and radiative cooling. Recent literature supports the importance of simple heat-rejection structures. Ahmed et al. demonstrated that radiative-cooling-assisted heat-pipe integration can reduce PV temperature and improve electrical efficiency [6]. Azirul et al. further showed that heatsink geometry strongly affects thermal-electrical performance in PVTE systems [7]. Utomo et al. reported improved performance for combined PV-TEG and heatsink panels operated with a dual-axis tracker [8]. In a related heat-transfer study, Ozbalci et al. found that plate-fin heatsinks substantially improved mean Nusselt number relative to an unfinned surface, outperforming pin-fin configurations under the tested conditions [9]. Durgam et al. also highlighted the practical suitability of aluminum-based heatsinks because of their lower density, lower cost, and easy machinability, even when compared against higher-conductivity alternatives [10].

Nevertheless, experimental studies on simple finned heatsinks in small-scale PV-TEG systems remain limited, while much of the existing literature focuses on more complex or actively cooled configurations. This research gap motivated the present study. The objective of this work was therefore to investigate systematically the effect of finned aluminum heatsinks on a hybrid PV-TEG system based on a 5 Wp monocrystalline PV panel and eight series-connected TEG modules per test section. The study specifically examined how the number of heatsink fins affects the TEG temperature difference and the overall electrical efficiency of the system. The working hypothesis was that increasing the number of fins would enlarge the convective heat-transfer area, maintain a lower cold-side temperature, increase ΔT, and ultimately improve the total power output of the hybrid PV-TEG system.

2 Methods

This study employed an experimental method to evaluate the effect of finned aluminum heatsinks on the output performance of a hybrid PV-TEG system.

2.1 System design and components

The experimental system consisted of two 5 Wp monocrystalline solar panels, sixteen TEC1-12706 thermoelectric modules, aluminum heatsinks, an Arduino Uno R3 microcontroller, INA219 current-voltage sensors, DS18B20 temperature sensors, an RTC module, and a MicroSD card module for automated data logging. Each PV panel was coupled with eight TEG modules connected in series in order to increase the total output voltage [11]. One panel was used as the PV-TEG reference system, while the second panel was used for the PV-TEG-heatsink configuration.

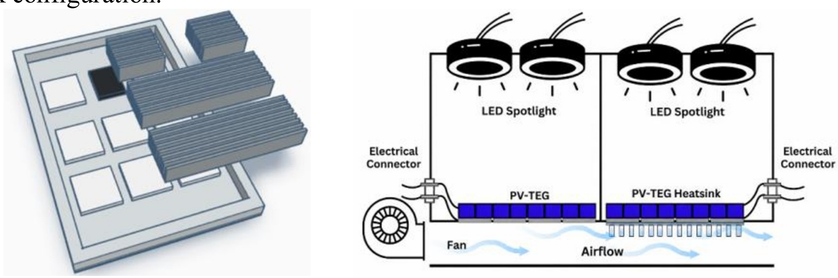

(a) (b)

Fig. 1. (a) Schematic design of the hybrid PV-TEG system equipped with finned aluminum heatsinks and (b) the corresponding experimental test arrangement under LED spotlight illumination

The TEG modules were mounted directly on the rear surface of the PV panel so that the hot side of each module was in thermal contact with the panel surface as shown in Figure 1. Thermal paste was applied at the panel-TEG interface and at the TEG-heatsink interface to reduce thermal contact resistance and improve heat transfer. The test rig was operated under controlled illumination using a 100 W LED spotlight. The lighting arrangement was designed to keep the incident radiation as uniform as possible over the panel surface during each test. The outer frame of the setup was lined with aluminum foil so that stray light was reflected back toward the PV surface. A fan was positioned near the heatsink to provide a consistent airflow over the cooling surface without disturbing the light distribution on the panel. Two aluminum finned heatsinks (Figure 2) were tested on the cold side of the TEG modules: a 4-fin heatsink and an 11-fin heatsink.

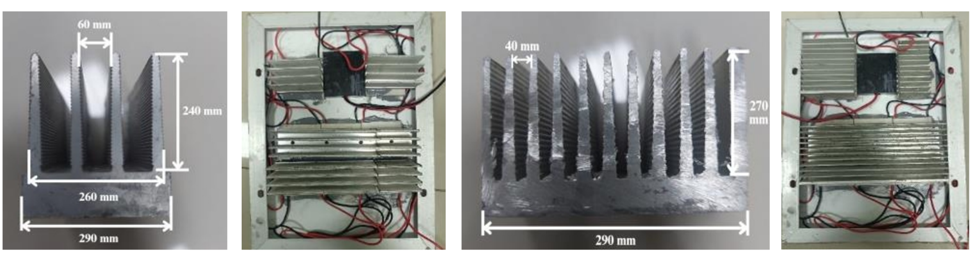

Fig. 2. Shape and Dimensions of 4-Fin and 11-Fin Aluminum Heatsinks, as well as Installation Positions in the PV-TEG System

2.2 Experimental setup and procedure

Before system testing, the sensors and major components were characterized. Two INA219 sensors were calibrated for voltage and current measurement against a Zoyi ZT102A digital multimeter using a 100 Ω, 10 W resistive load and a DC power supply. The input voltage was varied from 2 V to 20 V in 2 V increments. Eight DS18B20 temperature sensors were characterized by comparison with a mercury thermometer during gradual water heating over the temperature range of 39–79 °C, with three repeated measurements for each sensor.

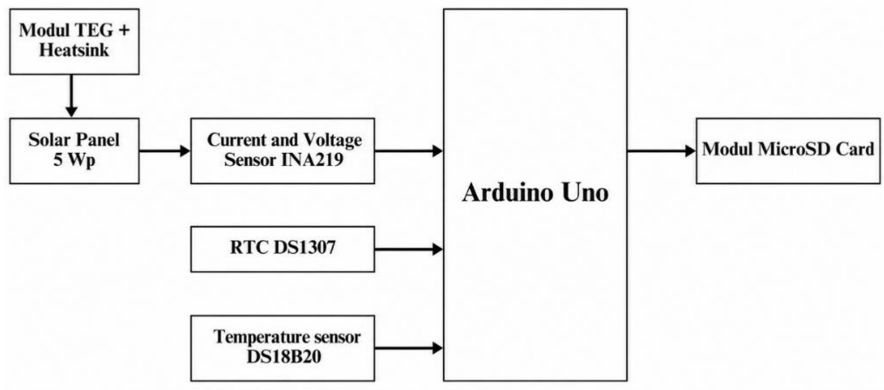

Fig. 3. Block diagram of the PV-TEG measurement system.

The main testing sequence comprised three configurations: without a heatsink, with a 4-fin heatsink, and with an 11-fin heatsink. During each experiment, the system was operated for 2 h, and temperature, current, and voltage data were recorded automatically every 2 min, yielding 60 data points per parameter for each configuration. Temperature sensors were placed on the PV surface, the hot side of the TEG, and the heatsink or TEG cold side to monitor the thermal response and to calculate the temperature difference across the TEG. Figure 3 showed the block diagram of the overall PV-TEG measurement system.

2.3 Data analysis

The collected data were screened for measurement inconsistencies and then processed to determine the electrical performance of the PV-TEG system. The overall efficiency and related parameters were calculated using the following relations:

$$\eta = \frac{P_{out}}{P_{in}} \times 100\% \quad (1)$$

$$P_{in} = G \times A \quad (2)$$

$$P_{out} = V \times I \quad (3)$$

$$P_{total} = P_{TEG} + P_{PV} \quad (4)$$

$$FF = \frac{V_m I_m}{V_{oc} \times I_{sc}} \quad (5)$$

$$\Delta T = T_H - T_C \quad (6)$$

where (G) is the irradiance in W/m², (A) is the PV surface area in m², (V) is voltage, (I) is current, (Vm) and (Im) are the voltage and current at the maximum power point, (Voc) is the open-circuit voltage, (Isc) is the short-circuit current, (TH) is the TEG hot-side temperature, and (TC) is the TEG cold-side temperature. The light intensity measured using a luxmeter is converted into W/m², with the conversion value of 1 Lux = 0.0079 W/m².

3 Result and discussion

3.1 Sensor and component characterization

The calibration results (Table 1 and Table 2) showed that the measurement system provided sufficiently reliable data for performance evaluation. For voltage measurement, INA219-1 yielded an error of 2.22% with an accuracy of 97.78%, whereas INA219-2 yielded an error of 3.60% with an accuracy of 96.40%. For current measurement, INA219-1 yielded an error of 1.81% and an accuracy of 98.19%, while INA219-2 yielded an error of 0.89% and an accuracy of 99.11%.

Table 1. Results of Data Processing for Voltage and Current Characterization of the INA219 Sensor

Voltage (V)			**Current (A)**		
Power Supply	**INA219-1**	**INA219-2**	**Power Supply**	**INA219-1**	**INA219-2**
2	2,05 ± 0,0115	2,05 ± 0,0120	0,01	0,0101 ± 0,000100	0,011 ± 0,00012
4	3,97 ± 0,0100	3,98 ± 0,0100	0,02	0,0226 ± 0,000153	0,0219 ± 0,000153
6	6,06 ± 0,0153	5,97 ± 0,0153	0,03	0,0334 ± 0,000153	0,0358 ± 0,000153
8	8,07 ± 0,0153	7,93 ± 0,0153	0,04	0,0453 ± 0,000208	0,0444 ± 0,000153
10	9,83 ± 0,0115	9,83 ± 0,0115	0,05	0,0499 ± 0,000153	0,0510 ± 0,000115
12	12,0 ± 0,0153	11,9 ± 0,0153	0,06	0,0624 ± 0,000153	0,0633 ± 0,000153
14	14,03 ± 0,0120	13,9 ± 0,0153	0,07	0,0709 ± 0,000173	0,0710 ± 0,000153
16	16,01 ± 0,0116	16,01 ± 0,0115	0,08	0,0846 ± 0,000153	0,0825 ± 0,000088
18	17,82 ± 0,0153	17,81 ± 0,0120	0,09	0,0935 ± 0,000219	0,0936 ± 0,000088
20	20,07 ± 0,0153	19,91 ± 0,0153	0,10	0,104 ± 0,000200	0,101 ± 0,000115

Table 2. Results of Error and Accuracy Calculations on the DS18B20 Temperature Sensor

Sensor DS18B20	**Error %**	**Accuracy %**
Sensor 1	2,86%	97,14%
Sensor 2	1,41%	98,59%
Sensor 3	2,71%	97,29%
Sensor 4	2,07%	97,93%
Sensor 5	2,84%	97,16%
Sensor 6	1,26%	98,74%
Sensor 7	1,31%	98,69%
Sensor 8	1,35%	98,65%

Based on Table 2, the DS18B20 sensors exhibited only very small errors, indicating that both the electrical and thermal sensing subsystems were suitable for real-time monitoring of the PV-TEG experiment.

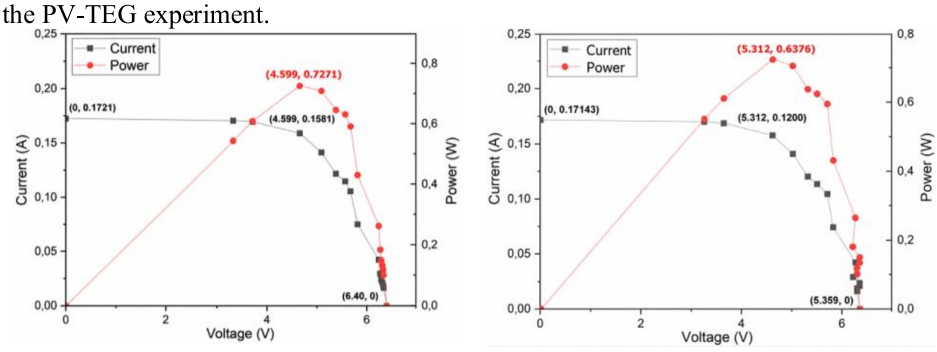

(a) (b)

Fig. 4. I–V and P–V curves characterization of the two 5 Wp monocrystalline PV modules of the PV modules: (a) Solar Panel 1, (b) Solar Panel 2

The two 5 Wp monocrystalline PV modules displayed the expected I–V and P–V characteristics as shown in Figure 4. At low voltage, the output current remained relatively stable, while near the open-circuit condition the current decreased rapidly toward zero. The P–V curves also showed a clear maximum power point. The second panel showed slightly better maximum-power characteristics than the first panel, and the corresponding (V_{oc}), (I_{sc}), (V_{mp}), (I_{mp}), and fill-factor (FF) values are as shown in Table 3.

Table 3. The values of Voc, Isc, Vmp, Imp and FF for each Solar Panel

Solar Panel	Voc (V)	Isc (A)	Vmp (V)	Imp (A)	Pmax (W)	Fill Factor
1	6,400	0,17210	4,599	0,1581	0,7271	69,39%
2	5,359	0,17143	5,312	0,1200	0,6376	66,01%

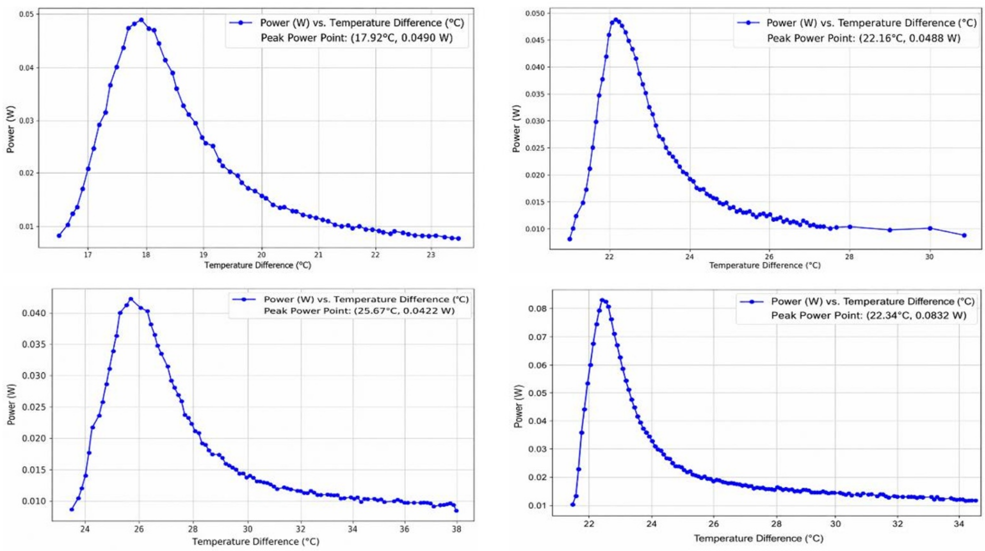

Fig. 5. Relationship between temperature difference, (ΔT), and TEG output power during TEG characterization

Based on Figure 5, the characterization of the TEG showed that output power increased with increasing temperature difference (ΔT), in accordance with the Seebeck effect. However, after reaching a peak, the power output began to decline even though the hot-side temperature continued to increase. This behavior indicates that if the cold side is not maintained at a sufficiently low temperature, the effective thermal gradient becomes unstable and thermoelectric performance deteriorates [12,13].

3.2 PV-TEG performance without a heatsink and with heatsinks (4-fin and 11-fin)

Figure 6 shows the experimental layout used to test the PV-TEG hybrid system under two configurations: without a heatsink and with a heatsink.

(a) (b) (c)

Fig. 6. (a) Measurement of LED spotlight light intensity, (b) Testing of the PV-TEG hybrid system, (c) Testing of the PV-TEG hybrid system with heatsink

For the reference PV-TEG configuration without a heatsink, the output-power trend was non-linear over time. Initially, the total output increased while the panel was still relatively cool. As the PV surface temperature rose and exceeded approximately 50 °C, the PV contribution decreased because of the thermal sensitivity of the photovoltaic module [14]. At later stages of the test, the TEG began to contribute more significantly as ΔT developed, partially compensating for the PV power drop. The results are presented in Figure 7 and Table 4. It should be noted that the average irradiance for the no-heatsink configuration was 593.32 W/m², whereas for the heatsink-assisted configurations it was 653.99 W/m². This difference in input irradiance introduces a limitation in directly comparing efficiencies across configurations. Ideally, irradiance should be maintained consistently to allow an apples-to-apples comparison of the heatsink effect. Using a PV area of 0.037975 m², the corresponding input power was 22.5315 W. The measured average electrical output was 0.1439 W, which gave an average system efficiency of 0.64%.

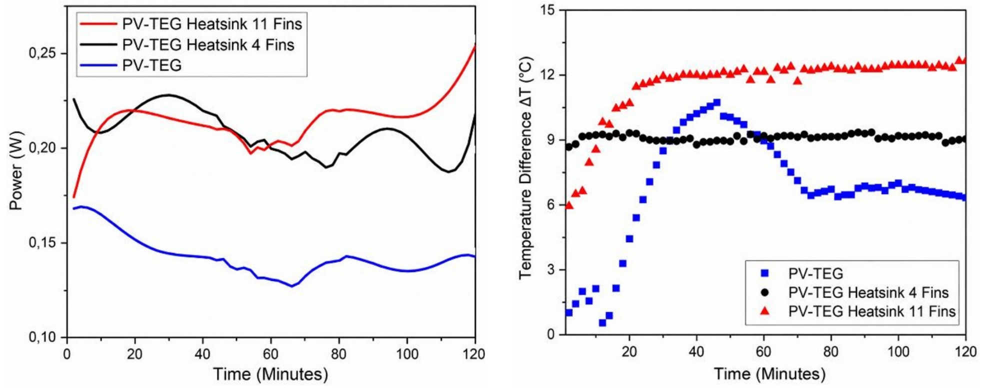

(a) (b)

Fig. 7. Comparative performance of the hybrid PV-TEG system for different cooling configurations: (a) output power as a function of time and (b) temperature difference as a function of time.

Table 4. Results of PV-TEG Testing with and without Heatsink

Configuration	Average irradiance (W/m²)	Average output power (W)	Average efficiency (%)	Average ΔT (°C)
No heatsink	593,32	0,1439	0,64	6,79
4-fin heatsink	653,99	0,2071	0,83	9,10
11-fin heatsink	653,99	0,2148	0,87	11,57

When finned aluminum heatsinks were added, both power output and temperature-difference performance improved. For the heatsink tests, the average irradiance reported in the source manuscript was 653.99 W/m², corresponding to an input power of 24.8352 W for the same active panel area.

The 4-fin heatsink configuration produced an average output power of 0.2071 W, an average efficiency of 0.83%, and an average ΔT of 9.10 °C. The 11-fin heatsink configuration produced the highest reported performance, with an average output power of 0.2148 W, an average efficiency of 0.87%, and an average ΔT of 11.57 °C. The maximum efficiencies reported for the 4-fin and 11-fin configurations were 1.02% and 1.06%, respectively.

The reported overall system efficiencies are considerably lower than the typical efficiency of monocrystalline PV modules (>15% under standard test conditions). This is mainly due to the non-optimal spectral characteristics of the 100 W LED light source used in the experiment, which does not replicate the full solar spectrum, and additional energy losses in the TEG modules, electrical wiring, and measurement system. These factors explain the low absolute efficiencies, although relative improvements due to heatsink integration remain valid.

The time-history comparison also indicated that the 11-fin heatsink maintained a lower cold-side temperature than the 4-fin design while the PV surface temperature remained in a similar range. As a consequence, the 11-fin design sustained a higher temperature difference across the TEG and generated a higher electrical output.

3.3 Comparative interpretation

A direct comparison of the three tested configurations shows that the use of finned aluminum heatsinks improved the reported performance of the hybrid PV-TEG system. Relative to the no-heatsink system, the average efficiency increased from 0.64% to 0.83% for the 4-fin heatsink and to 0.87% for the 11-fin heatsink. In absolute terms, this corresponds to gains of 0.19 and 0.23 percentage points, respectively. The increase in fin number also improved the heatsink-assisted configuration itself: based on the reported averages, the 11-fin design exceeded the 4-fin design by approximately 3.7% in average output power and by approximately 27.1% in ΔT.

This trend can be explained by the larger convective surface area provided by the greater number of fins. A larger finned area promotes more efficient heat rejection to the surrounding air, keeping the TEG cold side at a lower temperature. Because aluminum has high thermal conductivity and is practical for lightweight heat-sink fabrication, heat can be transferred effectively from the heatsink base to the fins and then dissipated to the environment [15]. The resulting increase in ΔT enhances thermoelectric power generation and improves the total electrical performance of the hybrid system.

4 Conclusion

The use of finned aluminum heatsinks in the hybrid PV-TEG system improved both output power and overall system efficiency by helping to maintain a lower TEG cold-side temperature and, consequently, a larger temperature difference across the thermoelectric modules. The source manuscript reports an average efficiency of 0.64% for the configuration without a heatsink, while the 4-fin and 11-fin heatsink configurations achieved 0.83% and 0.87%, respectively. The 11-fin heatsink yielded the highest average power output, 0.2148 W, together with the highest reported temperature difference, (ΔT = 11.57 °C). Overall, the results indicate that increasing the number of fins improves the thermal stability of the TEG cold side and enhances the electrical performance of the hybrid PV-TEG system. These findings support the use of simple finned aluminum heatsinks as a practical strategy for improving the performance of small-scale PV-TEG configurations.

This publication was funded by the Indonesia Endowment Fund for Education (LPDP) on behalf of the Indonesian Ministry of Higher Education, Science and Technology, and managed under the EQUITY Program (Contract Number 4308/B3/DT.03.08/2025 and B/284/UN39/HK.07.00/2025).

References

1. M.A. Fini, et al., Energy Convers. Manag. **265**, 115767 (2022). https://doi.org/10.1016/J.ENCONMAN.2022.115767
2. R. Kumar, et al., Appl. Therm. Eng. **227**, 120420 (2023). https://doi.org/10.1016/J.APPLTHERMALENG.2023.120420
3. F. Selimefendigil, et al., Sustainability **15**, 5424 (2023). https://doi.org/10.3390/SU15065424

4. S. Shittu, et al., Energy Convers. Manag. **207**, 112515 (2020). https://doi.org/10.1016/J.ENCONMAN.2020.112515
5. A. Wodołażski, et al., Materials **14**, 5800 (2021). https://doi.org/10.3390/MA14195800
6. S. Ahmed, et al., Appl. Energy **308**, 118363 (2022). https://doi.org/10.1016/J.APENERGY.2021.118363
7. A. Azirul, et al., Sci. Rep. **15**, 13586 (2025). https://doi.org/10.1038/s41598-025-97461-x
8. B.R. Utomo, et al., Energies **16**, 2658 (2023). https://doi.org/10.3390/EN16062658
9. O. Ozbalci, et al., Processes **10**, 1644 (2022). https://doi.org/10.3390/PR10081644
10. S. Durgam, et al., J. Phys. Conf. Ser. **2312**, 012016 (2022). https://doi.org/10.1088/1742-6596/2312/1/012016
11. K. N. Gonder, H. Rezk, Sustainability **13**, 3511 (2021). https://doi.org/10.3390/SU13063511
12. S. Ozbektas, et al., Heat Transfer **35**, 814–823 (2021). https://doi.org/10.2514/1.T6212
13. Y.H. Li, et al., IOP Conf. Ser. Mater. Sci. Eng. **292**, 012063 (2018). https://doi.org/10.1088/1757-899X/292/1/012063
14. M. E. Mliles, et al., Energy Harvest. Syst. **10**, 15–23 (2023). https://doi.org/10.1515/EHS-2022-0015/XML
15. V. Madhavadas, et al., IOP Conference Series: Earth and Environmental Science. **850**, 1–16 (2021). https://doi.org/10.1088/1755-1315/850/1/012029